Delft University of Technology

Joint Analysis and Reliability Test of Epoxy-Based Nano Silver Paste Under Different Pressure-Less Sintering Processes

Wang, Xinyue; Zeng, Zejun; Zhang, Guoqi; Zhang, Jing; Liu, Pan

DOI
10.1115/1.4053432

Publication date
2022

Document Version
Final published version

Published in
Journal of Electronic Packaging, Transactions of the ASME

Citation (APA)
Wang, X., Zeng, Z., Zhang, G., Zhang, J., & Liu, P. (2022). Joint Analysis and Reliability Test of Epoxy-Based Nano Silver Paste Under Different Pressure-Less Sintering Processes. *Journal of Electronic Packaging, Transactions of the ASME*, *144*(4), Article 041013. https://doi.org/10.1115/1.4053432

Important note
To cite this publication, please use the final published version (if applicable).
Please check the document version above.

Copyright
Other than for strictly personal use, it is not permitted to download, forward or distribute the text or part of it, without the consent of the author(s) and/or copyright holder(s), unless the work is under an open content license such as Creative Commons.

Takedown policy
Please contact us and provide details if you believe this document breaches copyrights.
We will remove access to the work immediately and investigate your claim.

This work is downloaded from Delft University of Technology.
For technical reasons the number of authors shown on this cover page is limited to a maximum of 10.

Green Open Access added to TU Delft Institutional Repository

'You share, we take care!' - Taverne project

https://www.openaccess.nl/en/you-share-we-take-care

Otherwise as indicated in the copyright section: the publisher is the copyright holder of this work and the author uses the Dutch legislation to make this work public.

Check for updates

Xinyue Wang
Faculty of Academy for
Engineering & Technology,
Fudan University,
No. 220, Handan Road,
Yangpu District,
Shanghai 200433, China
e-mail: 20210860007@fudan.edu.cn

Zejun Zeng
Faculty of Academy for
Engineering & Technology,
Fudan University,
No. 220, Handan Road,
Yangpu District,
Shanghai 200433, China
e-mail: 19210860052@fudan.edu.cn

Guoqi Zhang
Electronic Components,
Technology, and Materials,
Delft University of Technology,
Mekelweg 4,
Delft 2628 CD, The Netherlands;
Shenzhen Institute of Wide-Bandgap
Semiconductors,
Shenzhen 518131, China
e-mail: g.q.zhang@tudelft.nl

Jing Zhang
Heraeus Materials Technology Shanghai Ltd,
No. 1, Guangzhong Road,
Minhang District,
Shanghai 201108, China
e-mail: j.zhang@heraeus.com

Pan Liu[1]
Faculty of Academy for
Engineering & Technology,
Fudan University,
No. 220, Handan Road,
Yangpu District,
Shanghai 200433, China;
Yiwu Research Institute of Fudan University,
Building 5, Zhongfu Plaza,
Chengbei Road,
Yiwu City, Zhejiang Province 322000, China;
Research Institute of Fudan University in Ningbo,
901 Binhai Er Road, Hangzhou Bay New Area,
Ningbo, Zhejiang Province 315336, China
e-mail: panliu@fudan.edu.cn

Joint Analysis and Reliability Test of Epoxy-Based Nano Silver Paste Under Different Pressure-Less Sintering Processes

Recent years, the sintered silver paste was introduced and further developed for power electronics packaging due to low processing temperature and high working temperature. The pressure-less sintering technology reduces the stress damage caused by the pressure to the chip, improves reliability, and is widely applied in manufacturing. Currently, most existed studies are focused on alcohol-based sintered silver pastes while resins have been demonstrated to improve the bonding properties of solder joints. Hence, the performance and sintering mechanisms with epoxy-based silver paste need to be further explored. In this work, a methodology for multifactor investigation is settled on the epoxy-based silver paste to reveal the relationship between the strength and the different influence factors. We first analyzed the characteristics of commercialized epoxy-based silver paste samples, including silver content, silver particle size, organic composition, sample viscosity, and thermal conductivity. Samples were then prepared for shear tests and microstructure analysis under different pressure-less sintering temperatures, holding time, substrate surface, and chip size. Full factor analysis results were further discussed in detail for correlation. The influence factors were ranked from strong to weak as follows: sintering temperature, substrate surface, chip size, and holding time. Finally, a thermal cycling test was carried out for reliability analysis. Epoxy residues are one of the possible reasons, which result in shear strength decreasing exponentially. [DOI: 10.1115/1.4053432]

Keywords: power electronic packaging, epoxy-based nano silver paste, low-temperature joint technology, pressure-less sintering

1 Introduction

Power electronic devices based on wide band-gap semiconductor materials, such as silicon carbide (SiC) and Gallium nitride (GaN) [1], have been developed rapidly in decades, which are well-known for high working temperature, high frequency, and high power density applications [2,3]. Chips based on these materials are widely applied in automotive electronics [4], aerospace electronics [5], electric energy transducers [6,7], etc. With innovations in chip materials, chip designs, and device fabrications, demands keep rising for advanced packaging materials such as die-attach materials to fulfill harsh application conditions, improve thermal management capability, current carrying capacity, and achieve a long lifetime [8,9].

Lead-tin solder is the traditional die attach material under high temperatures (about > 350 °C) for power electronics packaging [10,11]. Due to the safety of lead and RoHS regulations, optimized lead-free solders such as Au-, Zn-, Bi-, and Sb-based alloys were developed as candidates for high-temperature die-attach materials [12,13]. The shear strength of joints formed by these alloy solders is approximately 20∼30 MPa [14]. However, when

[1]Corresponding author.

Contributed by the Electronic and Photonic Packaging Division of ASME for publication in the Journal of Electronic Packaging. Manuscript received June 19, 2021; final manuscript received December 14, 2021; published online February 1, 2022. Assoc. Editor: Kaushik Mysore.

 Copyright © 2022 by ASME

Downloaded from http://asmedigitalcollection.asme.org/electronicpackaging/article-pdf/144/4/041013/6875569/ep_144_04_041013.pdf by Bibliotheek Tu Delft user on 05 January 2023

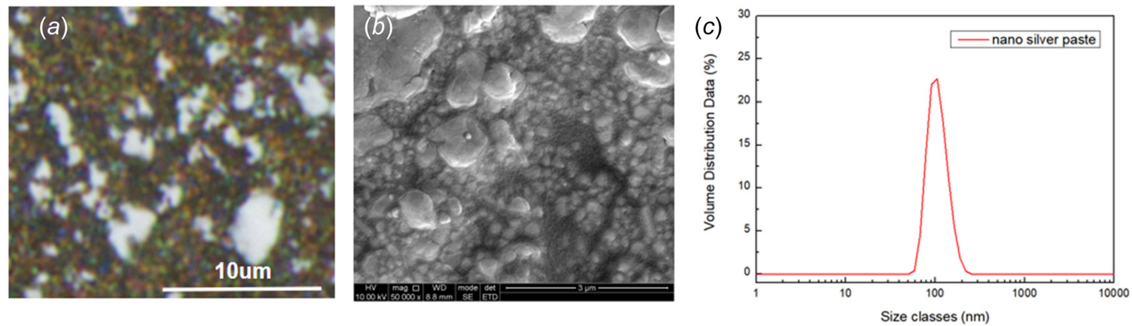

Fig. 1 The morphology of silver paste sample under (*a*) optical microscopy and (*b*) SEM; (*c*) dynamic light scattering analysis results of the diluted sample

the service temperature reaches 80% of the melting point of the solder (about > 150 °C), the creep deformation becomes serious and the joint reliability is damaged [15]. Therefore, new alternative die-attach materials with better thermal and electrical conductivity performance and high reliability have been further explored [16]. Meanwhile, altering organic additives is one effective approach to improve the performance of joints. Organic additives significantly influence the electrical conductance, mechanical characteristics, and reliability of the paste by influencing parameters such as viscosity and dispersion [17,18]. In order to combine the advantages of organic materials and solder alloys, more and more experts and scholars have paid attention to the research of epoxy-based solder paste to achieve higher strength joints [19–21] during past decades. Furthermore, solder paste with epoxy introduced as a matrix also alleviates the problem of short-circuiting caused by metallic whisker formation [22].

On the other hand, with the development of micro-and nanomaterials [23], silver (Ag) sintering is emerging as a promising solution for low-temperature joint technology [24]. Numerous studies have reported the excellent performance of these promising alternative approaches [25–33]. The main components of the paste are nano or micron Ag particles with high surface energy, dissolved by organic solvent for uniform distribution. Such pastes meet the environmental requirements of lead-free [34] solders. Unlike welding or soldering, Ag sintering technology is based on the transfer of solid materials through atomic diffusion driven by the reduction of total surface energy and interfacial energy [35]. Such a process occurs far below the melting point of the material and can be as low as 0.38 homologous temperature (>150 °C). Moreover, the sintered structure has the melting point of bulk silver (961 °C), and high conductivity, high heat conduction, creep resistance, and excellent ductility as well, which improves the reliability of the joints. However, most of the existing studies on sintered silver paste are focused on the alcohol-based solvent. There are few reports focused on epoxy-based sintered silver paste. Jung et al. fabricated various Ag-nanoparticle pastes containing different epoxy/binder percent weights (epoxy: 4.5, 9.0, 13.5, and 18 wt %) to investigate the effect on the bonding strength and electrical performance of multilayer ceramic capacitor components [36]. In their work, all samples were sintered under 250 °C for 15 min and the addition of epoxy at the moderate content from 9.0 to 13.5 wt % is desirable if considering both electrical and mechanical characteristics in electronic packaging. In conclusion, it remains to be explored that the performance and reliability of the epoxy-based sintered silver joints under different production processes, and specific mechanisms of action between resin and metal particles.

To promote the solidification and sintering of the paste to form joints, external energy is needed as a driving force. During the production process, pressure-assisted sintering and pressure-less sintering are both available. The pressure-assisted process will reduce the porosity but will also introduce residual stress into the chip, thus hindering the automated production process [15,37,38]. On the other hand, pressure-less sintering is a conventional connection method under normal pressure and driven by heat directly, or by the application of microwave radiation [39], infrared radiation [40], or laser radiation [41], which is the most economical method and is commonly applied among sintering. However, the disadvantage is that pressure-less sintering is not suitable for large chips due to the pores caused by evaporation and decomposition of solution during the sintering process, which will lead to the lack of reliability [42–44]. Therefore, to meet the application requirements of lower cost and higher efficiency in industrial mass production, it is of great significance to further optimize the technology pressure-less sintering.

In this work, we first analyzed the basic characteristics of the epoxy-based silver paste samples, including silver content, silver particle size, organic paste composition, sample viscosity, and thermal conductivity of the sintered sheets. A methodology was set for a multifactor investigation on silver paste, revealing the relationship between the strength and the influence of the factors. Based on the test methodology, samples of lead frame/silver paste/dummy chip were then prepared under different pressure-less sintering temperatures, holding time, substrate surface, and different chip sizes. Shear test, fracture observation based on optical microscopic, and cross section analysis based on scanning electron microscope (SEM)/energy dispersive spectroscopy (EDS) were applied for the joints. Then, characterization under the temperature cycling (−55∼150 °C, 2 cycles/h) was utilized for reliability analysis. The goal of this work is to identify the influence of critical pressure-less sintering processing parameters on joint reliability based on epoxy-based sintering pastes.

2 Materials and Methods

2.1 Materials. A commercialized sintered paste was selected since it was composed of epoxy and nanosilver particles. Due to the paste composition, the sample needs to be stored at −40 °C to avoid curing before application, thus ensuring the performance of the joints. The viscosity of the sample was 23.9 Pa·s, which was characterized through a rheometer test. Figure 1(*a*) showed the morphology and the size of silver particles under an optical microscope (1000×) observation. The silver paste was first coated on the silicon wafer. Compressed air was then applied to achieve a thin layer that was evenly distributed. After drying in the nitrogen cabinet for 24 h, the surface morphology of the particles was observed under a scanning electron microscope, as shown in Fig. 1(*b*). Most of the silver nanoparticles were in the shape of spherical with a protective coating. Micron-sized silver particles were also observed. To further analyze the diameter distribution of silver nanoparticles, a dynamic light scattering test by Zeta Potential Tester (ZEN3600, Malvern Company, Worcestershire, UK) was performed on the diluted solution, as shown in Fig. 1(*c*). It was found that the diameter of silver nanoparticles was normally distributed around 100 nm, which is consistent with the microscopic observation.

Second, Nicolet 380 (Thermo Nicolet Corporation, Waltham, MA) Fourier transform infrared spectroscopy (FTIR) was applied to study the solvent of silver paste. The solvent is important for

Downloaded from http://asmedigitalcollection.asme.org/electronicpackaging/article-pdf/144/4/041013/6875569/ep_144_04_041013.pdf by Bibliotheek Tu Delft user on 05 January 2023

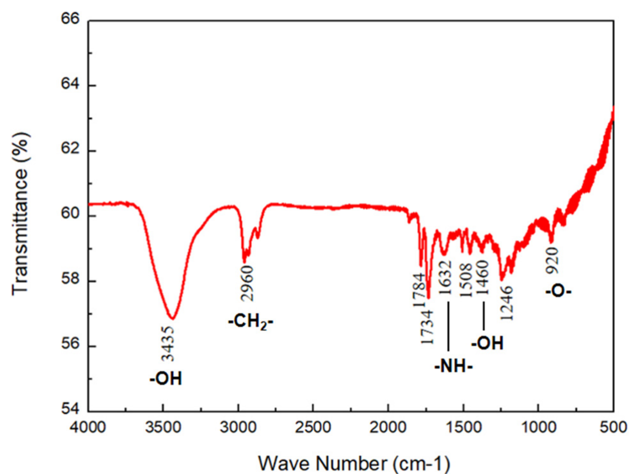

Fig. 2 Result of infrared analysis of silver paste sample

paste composition, since it scatters metal particles during dispensing, protects particles away from oxidation during sintering, and evaporates after the sintering process. Through the analysis of Fig. 2, hydroxyl groups, amine groups, and epoxy groups were found in the solvent. Therefore, the curing process of epoxy resin was carried out together with the sintering process. Meanwhile, amines and alcohols containing –OH (contained a large amount of active hydrogen), formed a hydrogen bond system in the liquid state, which may provide a protective effect on the surface with the high activity of nanoparticles.

Third, SDT-Q600 synchronous thermal analyzer produced by TA Instrument Company (New Castle, DE) was selected to analyze the thermal performance of the silver paste samples, thus further investigating the decomposition and volatilization process of the organic solvent system. During the test, the samples were heated up to 600 °C at the rate of 10 °C per minute under nitrogen protection, and the gas flow rate was 100 mL/min during the whole process. As shown in Fig. 3(*a*), the heating process of nanosilver paste was a continuous weight loss process. When heated up to 600 °C, the final weight loss was stabilized at 9.27 wt %, indicating that the silver content was around 90.73 wt %. Combined with the changing trend of differential scanning calorimetry (DSC) and differential thermal analysis (DTG) curves, the thermal weight loss process was divided into three parts as follows:

- The first stage was from room temperature to 130 °C. The DSC curve shifted downward significantly, indicating that organic solvents absorbed heat. The DTG curve remained stable, indicating that the system mass was unchanged. Therefore, the heat absorption in the first stage was caused by weak chemical endothermic fractures, such as hydrogen bonds between macromolecules of organic solvents.
- The second stage was 130∼250 °C. In this stage, the DSC curve formed a small exothermic peak around 189 °C, and the DTG curve formed a weight-loss peak. Therefore, the second stage was a process in which organic residues gradually volatilized under heat, and nanoparticles gradually contacted to form sintering necks and grew up to sintering tissues. As the surface activity between nanoparticles is extremely high, a high exothermic peak should be observed. However, such a peak did not show up in Fig. 3(*a*). Therefore, the heat released by the sintering of silver particles in the process was approximately equal to the heat flow during the endothermic process of organic volatilization and the destruction of a large number of chemical bonds between the surface protection groups of nanoparticles.
- In the third stage (after 250 °C), the DSC curve formed a heat absorption peak near 369.37 °C, while the DTG curve formed a large weight loss peak there. Therefore, the process was the volatilization and decomposition of organic residues and further densification of sintering tissues. The weight maintained stable afterward.

The thermal performance analysis was also investigated in the air atmosphere (Fig. 3(*b*)), which was similar to the actual condition of sintering experiments. The thermogravimetric analysis and the heat flow curve were similar compared to the results under nitrogen atmosphere in the range of low temperature (<300 °C). Therefore, the atmosphere almost plays no influence on the oxidation of organic solvent in low-temperature sintering. As shown in Fig. 3(*b*), in the range of 350∼550 °C, the heat was released due to the combustion or oxidative decomposition of organics based on the analysis of organic solvent.

Through the analysis of particle morphology, organic solvent, and thermal properties of the epoxy-based sintering paste samples in Sec. 2.1, the results provided a basis for the later experimental design and mechanism analysis.

2.2 Samples and Experiment Preparation.

The samples were prepared through (1) dispensing; (2) mounting; (3) sintering for later sintering experiments under different pressure-less processes, as shown in Fig. 4(*a*). Through these steps, we obtained the sintered samples of a sandwich structure with lead frames/silver paste/silicon-based dummy chips. As shown in Fig. 4(*b*), T0-220-3 L lead frames with pure copper surface and a 2∼3 μm electroplated silver surface were both chosen. Dummy chips with sizes of 2 mm × 2 mm × 0.25 mm and 4 mm × 4 mm × 0.25 mm were selected, respectively, to replace actual power chips. The back of the dummy chips has a silver coating with a thickness greater than 0.1 μm.

The reference process of the paste provided by the supplier (Fig. 5(*a*)) was as follows: heating from 25 °C to 130 °C for

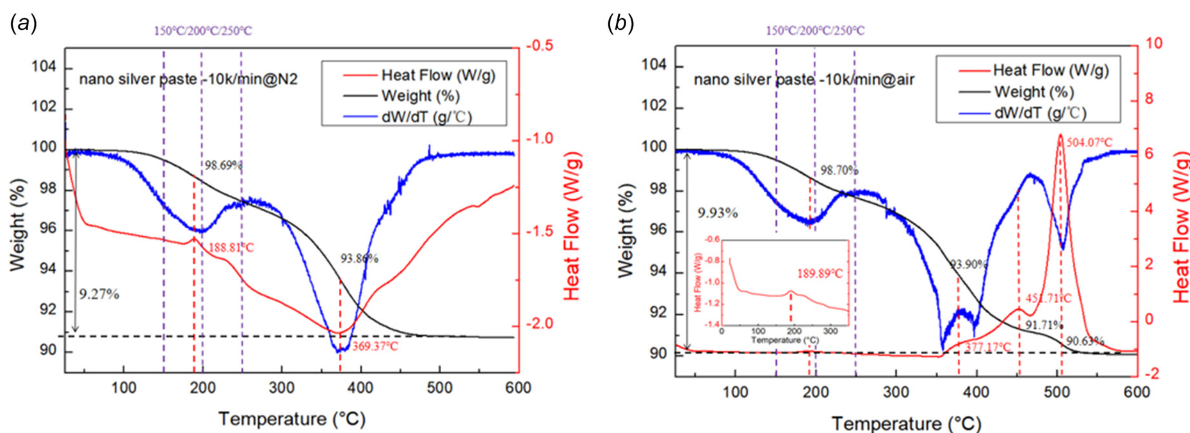

Fig. 3 Thermal performance analysis of the sample under (*a*) nitrogen and (*b*) air atmosphere

Downloaded from http://asmedigitalcollection.asme.org/electronicpackaging/article-pdf/144/4/041013/6875569/ep_144_04_041013.pdf by Bibliotheek Tu Delft user on 05 January 2023

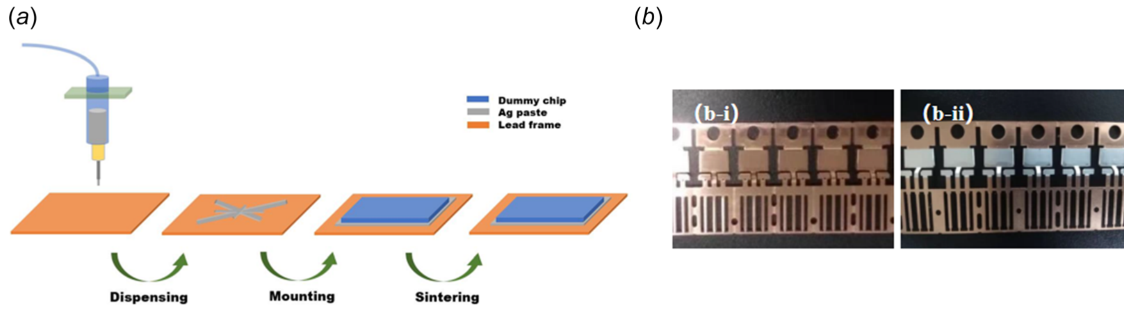

Fig. 4 (*a*) Schematic diagram of sintering sample preparation process and (*b*) sample preparation required items for sintered samples: (*b*-i) pure copper lead frame and (*b*-ii) silver-coated lead frame

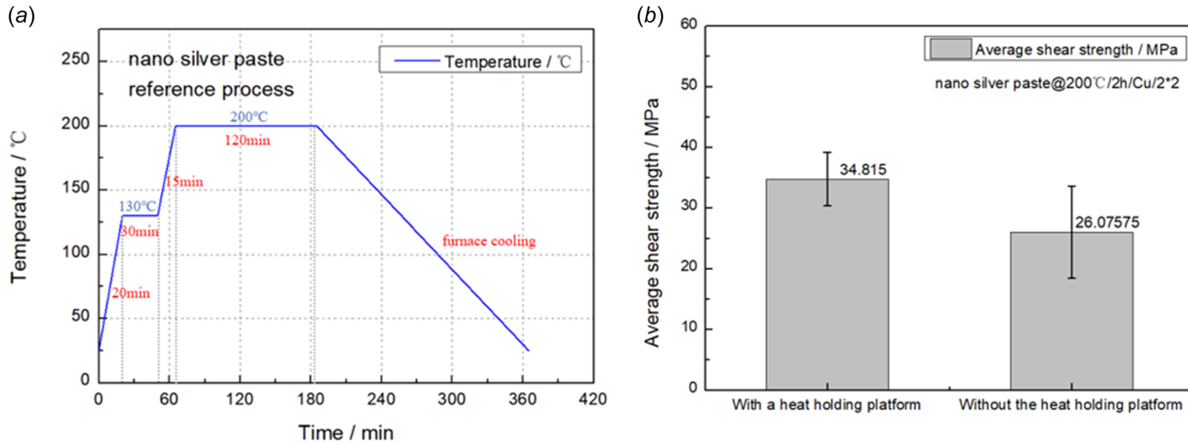

Fig. 5 (*a*) Reference temperature curve for sintering process and (*b*) result of the comparison of with or without insulation platform during the reference process

20 min, holding temperature for 30 min, heating to 200 °C for 15 min, holding temperature for 2 h, and then cooling with the furnace. To explore the influence of the presintering process, a group of comparative experiments was accomplished and the shear test was then compared, as shown in Fig. 5(*b*). The results showed that the presintering process helped the samples to significantly improve shear strength and stability. Therefore, the presintering process at 130 °C for 30 min was kept in the following experiments.

2.3 Test Methodology. To characterize the properties of epoxy-based silver paste samples, a series of tests were designed. The test route of the samples is presented in Fig. 6. First, we investigated the composition of the paste. SEM combined with dynamic light scattering was applied to observe the particles, and FTIR was utilized to analyze the organic part of the paste. Second, the thermal performance of the paste was explored through the DSC-DTG test. The first two steps are shown in Sec. 2.1. Then, sintered samples were prepared under different sintering processes and were compared by shear test, SEM/EDS, and optical microscope observation. Critical influence factors were analyzed, including sintering temperature, holding temperature, substrate surface, and chip size. To further investigate the importance of each influence factor, the range of each influence parameter was set as follows:

- *Sintering temperature (150 °C, 200 °C, 250 °C)*: We set the sintering temperature mainly based on the DSC test results. According to the DSC test results, there were obvious heat and weight changes of sinter pastes between 150 °C and 250 °C, which was also the temperature range of the conventional sintering process. Hence, the sintering temperature parameters were set as 150 °C, 200 °C, and 250 °C, respectively, in later experiments.
- *Holding time (1 h, 1.5 h, 2 h):* The suggested holding time (1 h) was selected as the reference process of the sample paste. In previous researches of our group, epoxy-based sinter pastes are difficult to reach complete curing during the low-temperature sintering process. Therefore, in this work, the holding time was set to be 1.5 h and 2 h for further comparison.
- *Substrate surface (pure copper, silver coated):* The copper substrate was chosen since it belongs to one of the most

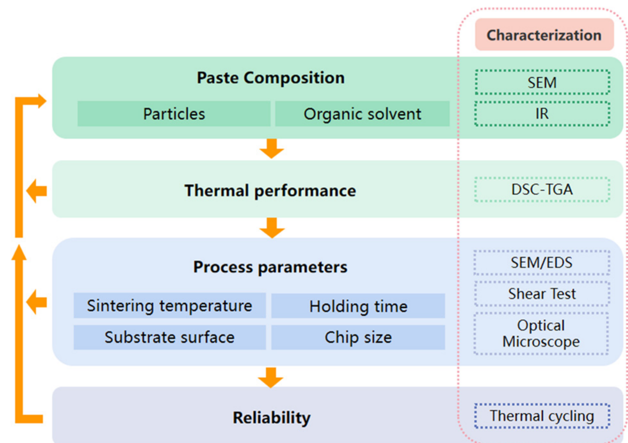

Fig. 6 The characterization test route of the silver paste sample and sintered samples

Downloaded from http://asmedigitalcollection.asme.org/electronicpackaging/article-pdf/144/4/041013/6875569/ep_144_04_041013.pdf by Bibliotheek Tu Delft user on 05 January 2023

Table 1 Comparison of thermal conductivity test results of the samples[a]

	ρ^{a} (g/cm^3)	C_p (J/(g·K))	Test point λ_1 (W/(m·K))	λ_2 (W/(m·K))	λ_3 (W/(m·K))	$\bar{\lambda}$ (W/(m·K))	SD
Epoxy based silver paste	10	0.214	8.182	8.155	8.19	8.176	0.018
Silver paste without epoxy	10	0.058	18.145	17.987	17.974	18.035	0.096

[a]Since the density of the sheet cannot be accurately measured for the time being, the thermal conductivity data in the following table were all calculated with the density of 10 g/cm^3.

widely applied choices in power electronics packaging. On the other hand, taking into consideration of the paste was composed of silver, silver-coated substrate was selected to compare the influence of the substrate surface.

- *Chip size (2×2 mm^2, 4×4 mm^2):* Such range basically covers the smallest power diodes chips (2×2 mm^2) up to the maximum chip size for high-quality pressureless sintering (4×4 mm^2). For chip sizes over 4×4 mm^2, the voids are obvious under high-resolution X-ray scans. Therefore, such two sizes of dummy chips were investigated.

Meanwhile, a full factor crossover experiment was designed by MINITAB software to facilitate subsequent data processing and analysis. A reliability test of thermal cycling was then carried out to evaluate the joints.

In summary, a methodology for testing silver paste samples was established, in which the effects of particle size distribution, viscosity, thermal properties, the influence of process parameters on joint performance and reliability are evaluated. Analysis was aimed to establish relationships between paste composition, thermal performance, process parameters, and reliability, which reveals the magnitude of influence of various factors on the quality of sintered joints.

3 Results and Discussions

3.1 Thermal Conductivity Test. The resin solidified in the sintering process coats the agglomerated silver particles. Since the thermal conductivity of resins is much lower than that of silver, it is expected to have a lower thermal conductivity of resin-based sintered silver paste. To confirm this, two kinds of commercial sintered silver samples were prepared for thermal conductivity examination. One is with resin and the other is without resin in composition. After screen printing on ceramic plates, samples were pressure-less sintered at their recommended temperatures. Then, flat cylinder samples were fabricated with approximately 6∼7 mm in diameter and 1∼2 mm in thickness. Subsequently, a laser thermal conductivity testing instrument (LFA 467) was applied to analyze thermal conductivity under (25 ± 5)°C, (30∼70)% relative humidity. The laser voltage was selected as 250.0 V with a pulse width of 0.30 ms. Because of intrinsic properties of pressure-less sintering such as porosity, organic residue, etc., the test value of thermal conductivity should be much lower than the actual value. Therefore, in this work, we compared the absolute value instead of test results, as listed in Table 1. It has been found that the average thermal conductivity of resin-based sintered samples is 0.45 times of the thermal conductivity of sintered samples without resin. Such a result confirms that the addition of resin has a significant negative effect on the thermal conductivity of sintered silver joints.

3.2 Analysis of Different Factors on Pressureless Sintering Performance. To evaluate the shear strength of sintered joint structures, Nordson's DAGE4000 shear instrument was utilized in later experiments.

A field emission scanning electron microscope (FEI F50) was applied to analyze the cross section of the samples. After obtaining the scanning electron microscope pictures of the cross section of the samples, IMAGEJ software was utilized to convert them into a binary-value graph to obtain the porosity of the sintered silver layer.

3.2.1 Sintering Temperature. Different sintering temperature impacts the connection properties of silver paste, as shown by the temperature curves of experiments in Fig. 7(*a*). Dummy chips (2×2 mm^2) and lead frames with copper substrate were chosen. Through the shear test and porosity analysis (Fig. 7(*b*)), as the temperature rose from 150 °C to 250 °C, the shear strength rose from 5.339 MPa to 58.180 MPa, while the porosity of the silver paste samples decreased from 22.25% to 12.86%. Through the microstructure analysis (Fig. 7(*c*)), the sintered aggregates were gradually densified to form a porous network interconnection structure. Meanwhile, the fracture patterns were changed with the increase in temperature. The sample showed obvious adhesion failure on the substrate at 150 °C. At 200 °C, the adhesive failure on the substrate was the dominant failure mode, and cohesive failure just occurred at the edge. When the sintering temperature was setup to 250 °C, a large area occurred cohesive failure in the middle part, while the substrate was surrounded by cohesive failure, and chip cohesive failure mode also occurred. Therefore, the sintered joints have a strong bonding at low temperatures. With the increase of temperature, the bonding strength significantly increased, which lead to the change of the failure mode. To detail study the mechanism of this process, EDS was planned to analyze the carbon content of the samples. The scanning test was carried out from the copper substrate to the sintered layer. In this work, the data of 4.5–8 μm were chosen for analysis because this part was at the middle of the sintered layer. First, the scanning signal was denoised. Fifty data points were taken as a processing window and the Savitzky–Golay method was chosen to calculate. Smoothed lines were then obtained, as shown in Fig. 7(*d*). For better comparison, we integrate the signal strength inside the sintered layer. In this experiment, the curve integral at 250 °C was 54.82, which was 13.66% lower than the 63.49 calculated by the curve integral at 200 °C. It indicates that higher temperature has a significant effect on reducing the carbon content of the sintering layer, which is beneficial to the decomposition of organic residues such as resin.

3.2.2 Holding Time. Holding time refers to the length of maintaining temperature time after the furnace gradually rises to the sintering temperature. Different holding time also affects the performance of joints. Therefore, different temperature curves were set as illustrated in Fig. 8(*a*). As shown in Fig. 8(*b*), with the extension of the sintering time, the mechanical property of the samples held for 1 h and 1.5 h remained similar. However, the shear strength of the joints increased to 34.815 MPa after being held for 2 h. Through the porosity analysis, it showed that the microstructure evolution of the sintered silver layer was not obvious. Moreover, the porosity did not change significantly (around 20%). On the other hand, as shown in Fig. 8(*c*), adhesion fracture was the main fracture mode on the substrate after being held for 1 h and 1.5 h, but it changed to cohesion fracture after being held for 2 h. For the carbon contents analysis, the same method described in Sec. 3.2.1 was applied. Through the results of Fig. 8(*d*), the curve integral of the sample held for 1 h was 63.95, which was approximately equal to the result of the sample

Downloaded from http://asmedigitalcollection.asme.org/electronicpackaging/article-pdf/144/4/041013/6875569/ep_144_04_041013.pdf by Bibliotheek Tu Delft user on 05 January 2023

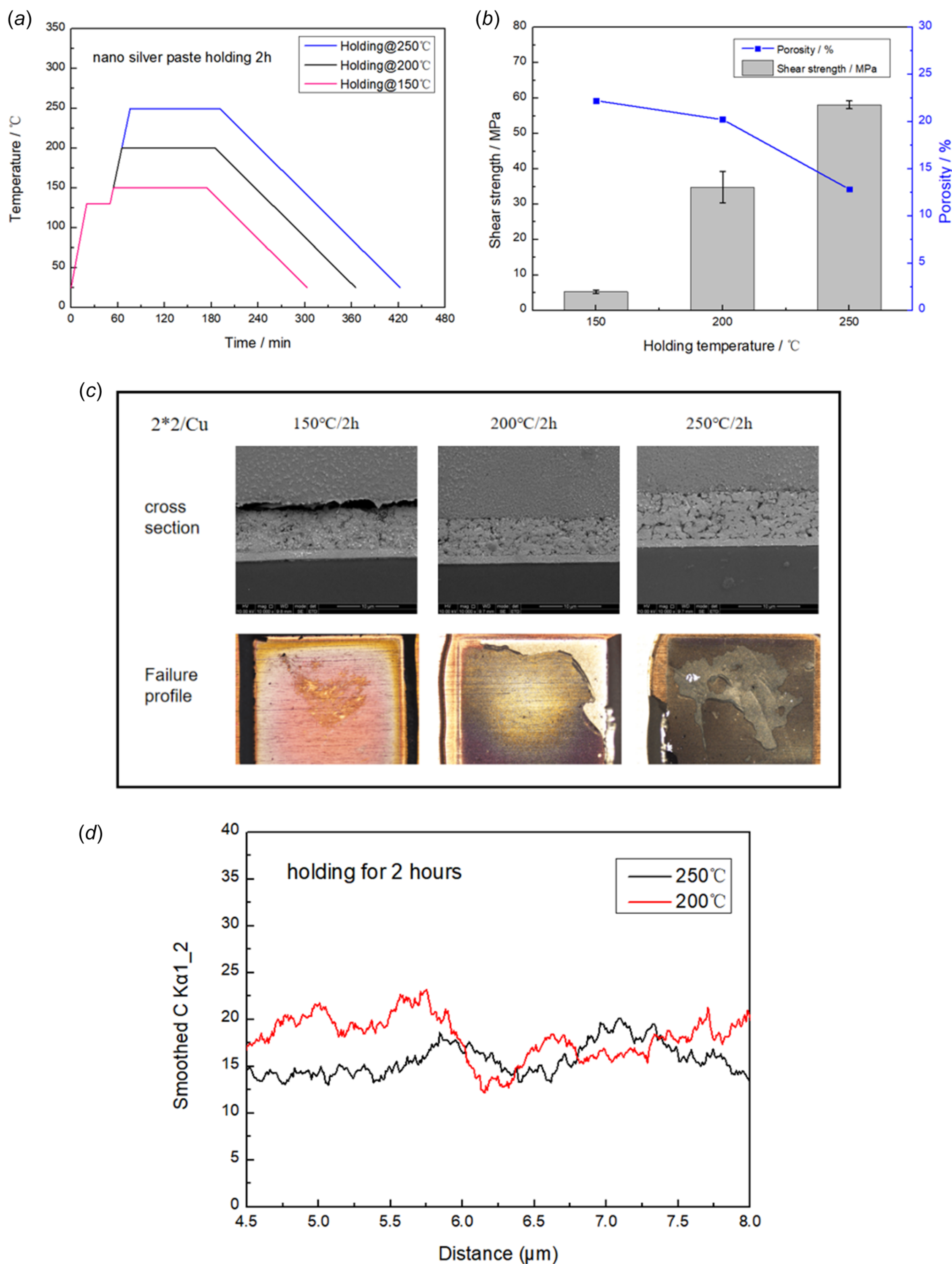

Fig. 7 **(*a*) Process curve under different sintering temperature; (*b*) results of shear test and porosity analysis; (*c*) microstructure analysis after holding at 150 °C,200 °C, 250 °C; and (*d*) EDS analysis of C content after holding at 200 °C, 250 °C**

held for 2 h (63.50). It indicates that the holding time has little effect on the contents of organic residues such as resin.

3.2.3 Substrate Surface. Substrate materials affect the performance of chip connections. Common substrate surfaces are Cu, Ag, Au, and so on. In this work, the pure copper substrate and silver-coated substrate are compared. The difference between the diffusion of copper and silver atoms and that of silver atoms is the main factor that leads to the difference in connection properties. As shown in Fig. 9(*a*), the shear strength of the sintered samples on the silver-coated substrate was 25.2 MPa at 200 °C for 2 h, which was a 27.59% decrease obtained on the pure copper substrate (34.8 MPa) under the same condition. The porosity of the sintered silver layer of the nanosilver paste sample was only 9.83% on the silver substrate, which was a 10.41% decrease on the pure copper substrate (20.24%).

The shear fracture mode changed from the failure dominated by adhesion fracture mode at the substrates to the cohesive fracture

Downloaded from http://asmedigitalcollection.asme.org/electronicpackaging/article-pdf/144/4/041013/6875569/ep_144_04_041013.pdf by Bibliotheek Tu Delft user on 05 January 2023

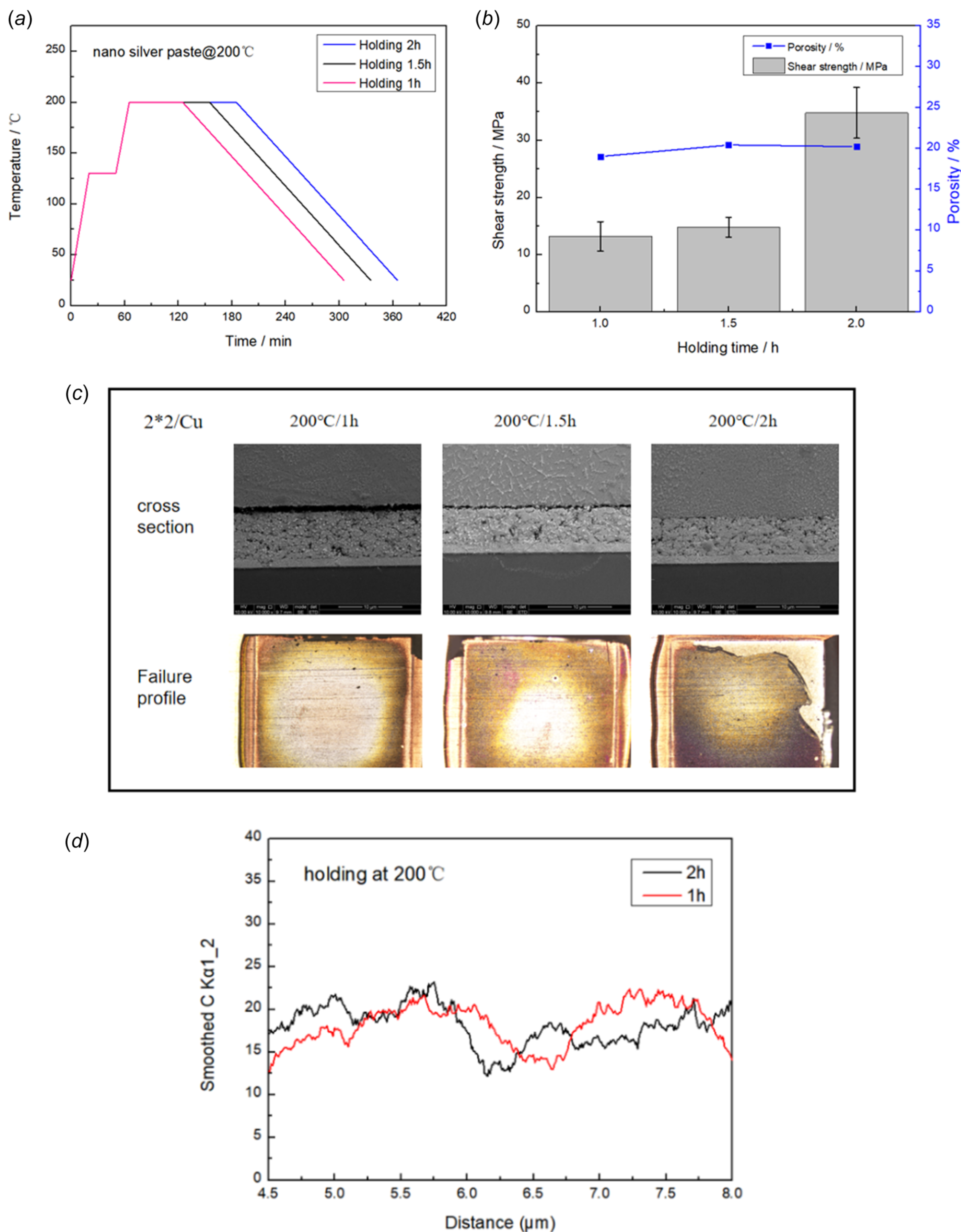

Fig. 8 **(*a*) Process curve under different holding time, (*b*) results of shear test and porosity analysis, (*c*) microstructure analysis after holding 1 h, 1.5 h, 2 h, and (*d*) EDS analysis of C content after holding at 1 h, 2 h**

failure mode. Microstructure analysis was carried out through SEM/EDS analysis, as shown in Fig. 9(*b*). It is clear that the sintered structure of the silver-coated substrate showed a lower porosity than that of the pure copper substrate. As for the 27.59% reduction of shear strength of the samples on a silver-coated substrate, it is speculated that the dominant factor is the change of shear fracture mode. This may be due to the brittle fracture of the intermetallic compounds in the copper-silver diffusion layer that occurs on the copper substrate. While for the result of EDS element analysis on the silver-coated substrate, due to the high activity of nanosilver particles and quicker diffusion of the silver-coated layer, it evolved into a structure without pores. Such a structure led to the fracture occurring inside the sintered silver layer. Hence, due to the low hardness of silver and the low shear strength of ductile fracture, the structure tended to lump silver had a decrease in shear strength.

3.2.4 Chip Size. The size of the chip impacts the sintering process, especially for pressure-less sintering. The organic solvent is decomposed and volatilized into gas during the heating process. As the chip size increases, the gas inside will be more difficult to exhaust. This will lead to the generation of sintered pores, which

Downloaded from http://asmedigitalcollection.asme.org/electronicpackaging/article-pdf/144/4/041013/6875569/ep_144_04_041013.pdf by Bibliotheek Tu Delft user on 05 January 2023

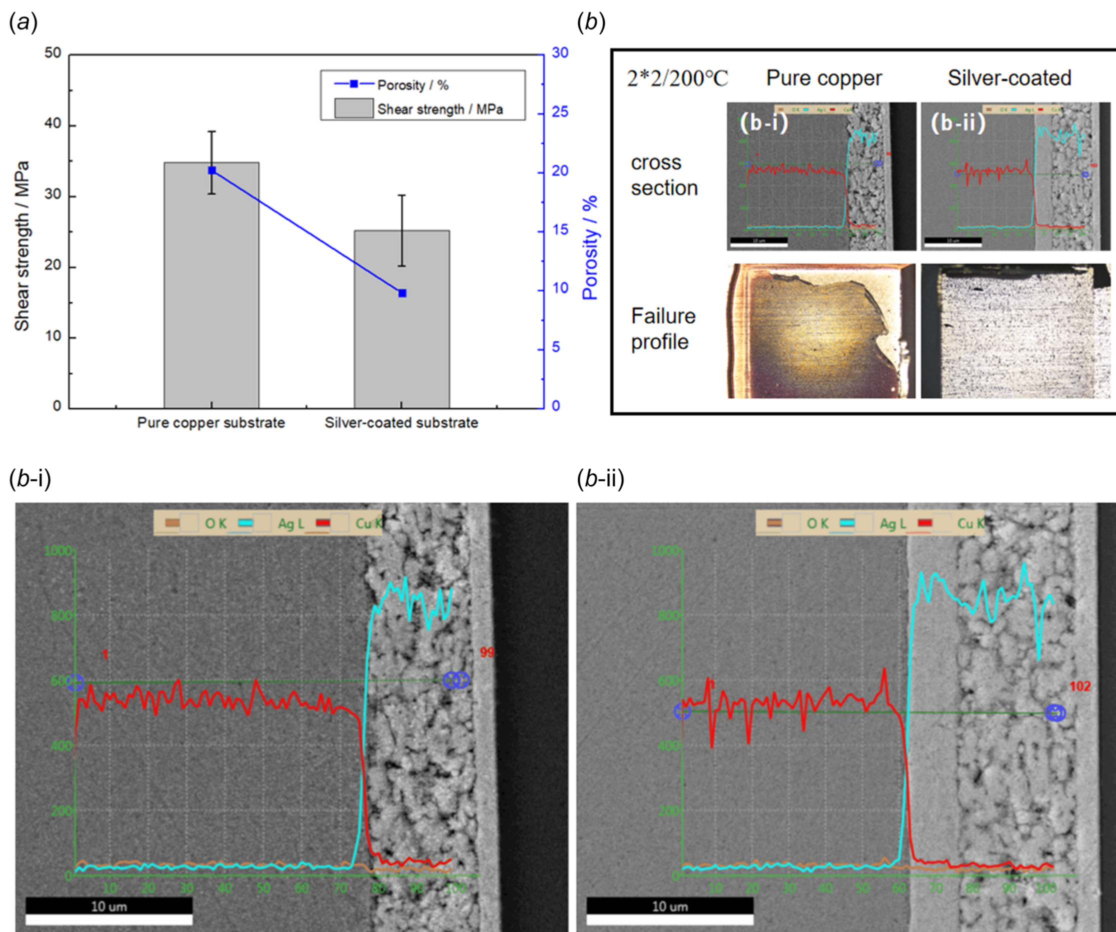

Fig. 9 Results of (*a*) shear test and porosity analysis and (*b*) microstructure analysis on different substrate materials

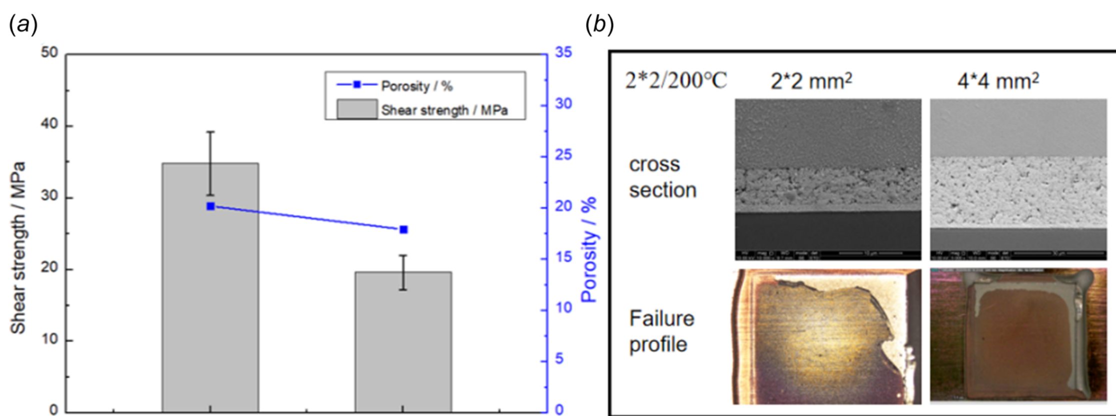

Fig. 10 Results of (*a*) shear test and porosity analysis and (*b*) microstructure analysis on different chip size

are negative to the reliability of the joints. In this work, chips including the size of $2 \times 2\,\text{mm}^2$ and $4 \times 4\,\text{mm}^2$ were chosen. All samples were compared under the reference sintering process. The obtained data results are shown in Figs. 10(*a*) and 10(*b*). The shear strength of the sintered sample with a $4 \times 4\,\text{mm}^2$ chip was 19.6 MPa under 200 °C for 2 h, which was lower than the 34.8 MPa obtained with a $2 \times 2\,\text{mm}^2$ chip. The porosity of the sintered silver layer under a $4 \times 4\,\text{mm}^2$ chip was only 17.95%, which was a 2.29% decrease under a $2 \times 2\,\text{mm}^2$ chip (20.24%). The values of porosity were close.

According to the microstructure analysis, the shear fracture mode of the silver paste did not change significantly. However, the holes in the sintered tissue increased significantly. This was caused by the larger amount of gas leakage during the sintering process when the chip was enlarged. It is estimated that the holes led to a decrease in shear strength.

3.2.5 Full Factor Analysis. Through the discussion above, the influence of these variables on the performance of pressure-less sintering has been recognized. However, the strength of each factor is not clear yet. Therefore, the analysis of the interactions between these variables was also designed in this work. The results of the designed multifactor level experiments were recorded in Table 2 below. Unfortunately, due to the limitation of

Downloaded from http://asmedigitalcollection.asme.org/electronicpackaging/article-pdf/144/4/041013/6875569/ep_144_04_041013.pdf by Bibliotheek Tu Delft user on 05 January 2023

Table 2 Full-factor experimental test results

	Substrate surface	Chip/mm^2	Sintering temperature/°C	Holding time/h	Average shear strength/MPa	Variance
1	Cu	2 × 2	200	2	34.815	4.426
2	Cu	4 × 4	200	2	19.621	2.387
3	Ag	2 × 2	200	2	25.208	5.041
4	Cu	2 × 2	200	1.5	14.817	1.745
5	Cu	4 × 4	200	1.5	16.435	2.236
6	Ag	2 × 2	200	1.5	32.854	2.265
7	Cu	2 × 2	200	1	13.191	2.554
8	Cu	4 × 4	200	1	11.557	3.350
9	Ag	2 × 2	200	1	32.048	5.002
10	Cu	2 × 2	150	2	5.339	0.498
11	Cu	4 × 4	150	2	2.864	0.499
12	Ag	2 × 2	150	2	16.008	1.407
13	Cu	2 × 2	150	1.5	5.408	0.278
14	Cu	4 × 4	150	1.5	2.922	0.168
15	Ag	2 × 2	150	1.5	13.264	1.723
16	Cu	2 × 2	150	1	4.339	0.230
17	Cu	4 × 4	150	1	3.177	0.184
18	Ag	2 × 2	150	1	12.583	1.625
19	Cu	2 × 2	250	2	58.180	1.109
20	Cu	4 × 4	250	2	42.762	1.833
21	Ag	2 × 2	250	2	54.365	1.297
22	Cu	2 × 2	250	1.5	61.580	2.150
23	Cu	4 × 4	250	1.5	33.594	1.088
24	Ag	2 × 2	250	1.5	69.840	1.948
25	Cu	2 × 2	250	1	76.580	3.179
26	Cu	4 × 4	250	1	37.792	1.953
27	Ag	2 × 2	250	1	68.582	3.099

the size of the silver-coated substrate in the actual experiment, the data of larger chips (4 × 4 mm^2) on the silver-coated substrate were not covered.

Minitab software was applied to analyze the results. The typical graphs were obtained and discussed in the following, respectively:

- Figure 11(*a*) presented the analysis of pressure-less sintering process conditions (temperature/time). The shear strength of the silver paste sample was improved with the increase of temperature, while the holding time had little influence on it. However, with the increase of sintering temperature, the influence of other conditions, such as substrate surface and chip size, on the connection strength of sintered samples will increase. In conclusion, extending the temperature holding time may reduce the influence of these factors.
- The variation trend in Fig. 11(*b*) presented the comprehensive influence degree of different factors on the connection strength under pressure-less sintering. The sintering temperature was the main driving force of the diffusion interconnection of silver particles, which had a significant impact on the connection strength of samples, followed by the factors of chip size and substrate surface. The effect of chip size and substrate surface type was similar. Holding time had an unapparent influence. It is also proved that the high activity of nanoparticles, which will effectively reduce the time of diffusion.
- Statistical analysis was conducted on the cross-influence of various factors considered in the experiment, with the detailed results exhibited in Fig. 11(*c*). The analysis diagram of existing data indicated that (1) the average connection strength of samples on a silver substrate was better than that on a copper substrate, (2) the connection effect of a small chip was better than that of a large chip, (3) higher sintering temperature will bring stronger sintering bonding strength, and (4) the change of holding time did not lead to significant results fluctuation.

3.3 Thermal Cycling Reliability Analysis. A thermal cycling test was carried out under the standard of JESD22-A10. The temperature range of the test was from −55 °C to 150 °C and the test condition was 2 cycles/h. Sintered samples (four samples/group) were taken out every 25 h for the shear test group by the group after 50 h. The variation trend of average shear strength with test time is shown in Fig. 12. The average shear strength of the samples decreased exponentially after the beginning of the thermal cycling test and stabilized at about 8.5 MPa. Subsequently, the average shear strength began to decline slowly after 125 h and less than 3 MPa after 225 h. Based on the analysis above, although the initial shear strength of the silver paste samples under the reference process was excellent, its reliability was insufficient under the long-term temperature cycling, which may be due to the content of the resin in the solvent. As shown in the results of EDS analysis of carbon before, epoxy residues were identified within the sintered silver layer. Epoxy resin is conducive to the improvement of shear strength, however, the residual resin after curing will aggravate the mismatch of the thermal expansion coefficient between the polymerized sintering layer and the substrate during the thermal cycle. They will reduce the reliability. Future work is needed to develop a kind of solvent to reduce the thermal expansion coefficient mismatch between the interface and be suitable for reliability.

4 Conclusions

This work presents an overall analysis of the materials, process, and reliability of an epoxy-based nanosilver sintering paste. First, the methodology of development and evaluation of silver paste is put forward according to the design of experiments. The composition of silver paste determines its thermal performance, which guides the regulation of process parameters. The properties of sintered samples provide further feedback for the composition development of silver pastes. Second, the quality of sintered joints was analyzed and the influence of the factors are ranking as sintering temperature, chip size, substrate surface, and holding time. The sintering temperature of nanosilver paste is the main driving force for the diffusion interconnection of silver particles, which has a significant influence on the connection strength of samples. The higher the temperature is, the better the connection strength will

Downloaded from http://asmedigitalcollection.asme.org/electronicpackaging/article-pdf/144/4/041013/6875569/ep_144_04_041013.pdf by Bibliotheek Tu Delft user on 05 January 2023

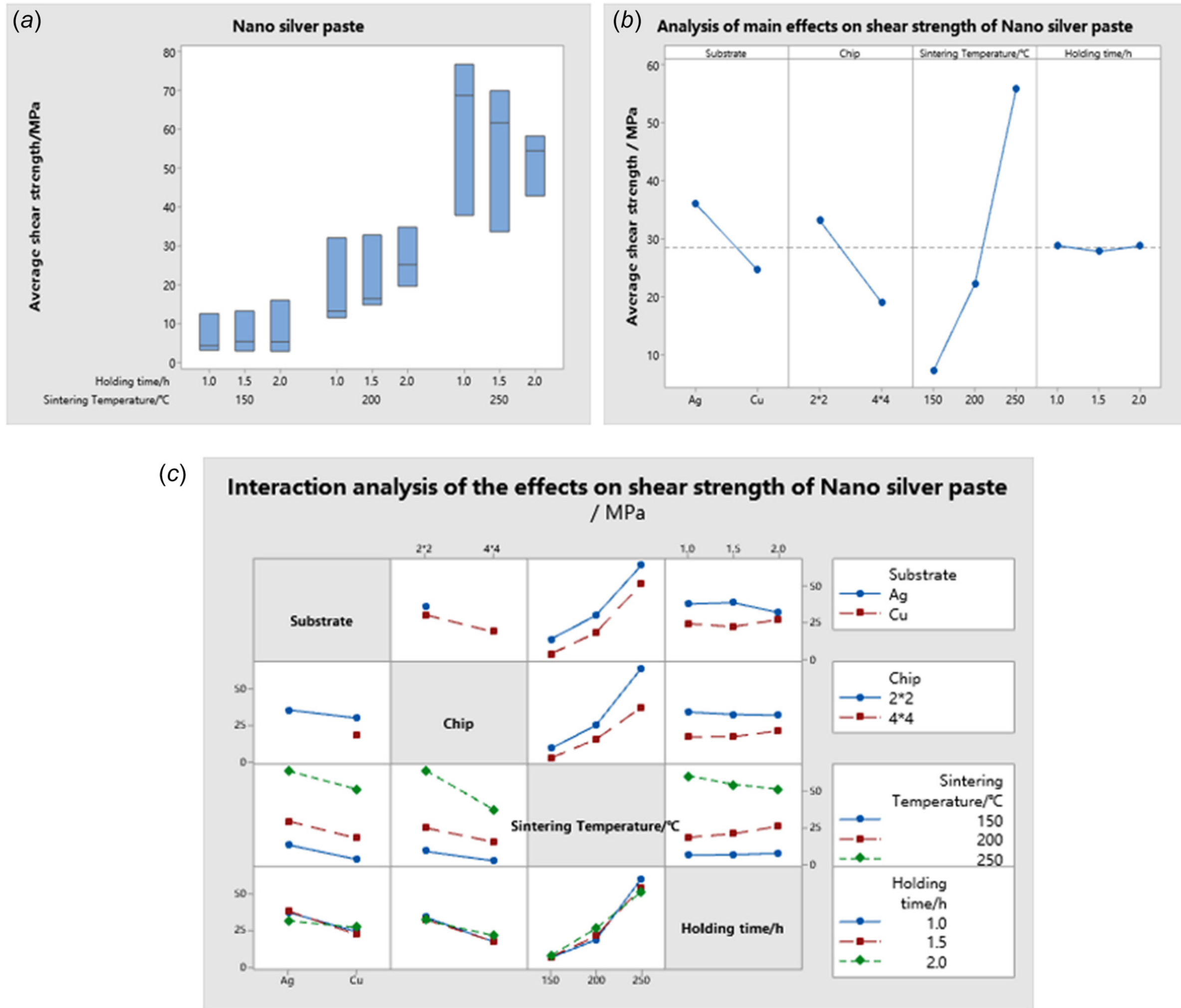

Fig. 11 The results based on MINITAB software: (*a*) the analysis of pressure-less sintering process conditions (temperature/time), (*b*) the analysis of main effects on shear strength, and (*c*) interaction analysis of the effects on shear strength

be. The effect of chip size under experimental conditions was similar to that of substrate type. The least significant effect is the duration of heat preservation. Third, the reliability of the sintered samples under the long-term thermal cycling test was analyzed. The shear strength decreased exponentially at the beginning and then stabilized at 8.5 MPa before falling to 3 MPa at 225 h, which may be due to the coefficient of thermal expansion mismatch aggravated by epoxy resin residues.

In terms of practical experiments, this work focuses on the mechanical properties after pressure-less sintering. Future work is planned to develop a high-quality epoxy-based pressure-less sintering paste by various hardeners, binders, and capping agents for high shear strength, good electrical and thermal conductivity, and a long lifetime for power applications.

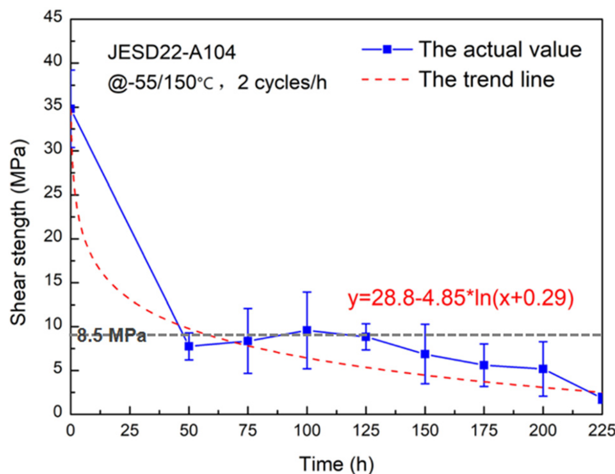

Fig. 12 Result of thermal cycling test

Acknowledgment

The authors sincerely appreciate the guidance from engineers, Mr. Leric Ji and Mr. Steven Mo from Heraeus Materials Technology Shanghai Ltd., and the support from Mr. Ke Li, a graduate student from the Department of Materials Processing and Engineering in Harbin University of Science and Technology, and Mr. Zhoudong Yang, a graduate student from Laboratory of Advanced Materials in Fudan University, respectively.

Funding Data

- Key-Area Research and Development Program of Guangdong Province (Grant No. 2020B010170002; Funder ID: 10.13039/501100007162).
- Science and Technology Innovation Base of Shanghai Municipal Science and Technology Commission, Shanghai SiC Power Device Engineering and Technology Research

Downloaded from http://asmedigitalcollection.asme.org/electronicpackaging/article-pdf/144/4/041013/6875569/ep_144_04_041013.pdf by Bibliotheek Tu Delft user on 05 January 2023

Center, Fudan University (Grant No. 19DZ2253400; Funder ID: 10.13039/501100003347).
- Fudan University-Heraeus cooperation project (Grant No. 20549; Funder ID: 10.13039/501100003347).

References

[1] Fu, L., Xuan, Z., Scott, M., Yao, C., and Wang, J., 2014, "The Evaluation and Application of Wide Bandgap Power Devices," International Transportation Electrification Asia-Pacific (ITECAP), Beijing, China, Aug. 31–Sept. 3, pp. 1–5.
[2] Jin, H., Li, Q., Lan, Z., Zeng, X., and Rui, Y., 2016, "Review of Wide Band-Gap Semiconductors Technology," MATEC Web Conf., **40**(01006), p. 01006.
[3] Rodriguez, M., Zhang, Y., and Maksimovic, D., 2014, "High-Frequency PWM Buck Converters Using GaN-on-SiC HEMTs," IEEE Trans. Power Electron., **29**(5), pp. 2462–2473.
[4] Gonzalez, J. O., Wu, R., Jahdi, S., and Alatise, O., 2020, "Performance and Reliability Review of 650 V and 900 V Silicon and SiC Devices: MOSFETs, Cascode JFETs and IGBTs," IEEE Trans. Ind. Electron., **67**(9), pp. 7375–7385.
[5] Perdikakis, W., Scott, M. J., Yost, K. J., Kitzmiller, C., Hall, B., and Sheets, K. A., 2020, "Comparison of Si and SiC EMI and Efficiency in a Two-Level Aerospace Motor Drive Application," IEEE Trans. Transport. Electrification, **6**(4), pp. 1401–1411.
[6] Bayram, F., Gajula, D., Khan, D., and Koley, G., 2020, "Investigation of AlGaN/GaN HFET and VO(2)Thin Film Based Deflection Transducers Embedded in GaN Microcantilevers," Micromachines, **11**(9), pp. 1–12.
[7] Li, X., Pu, T., Li, L., and Ao, J.-P., 2020, "Enhanced Sensitivity of GaN-Based Temperature Sensor by Using the Series Schottky Barrier Diode Structure," IEEE Electron Device Lett., **41**(4), pp. 601–604.
[8] Ghimire, P., De Vega, A., Beczkowski, S., Rannestad, B., Munk-Nielsen, S., and Thogersen, P., 2014, "Improving Power Converter Reliability: Online Monitoring of High-Power IGBT Modules," IEEE Ind. Electron. Mag., **8**(3), pp. 40–50.
[9] Luo, H., Chen, Y., Sun, P., Li, W., and He, X., 2016, "Junction Temperature Extraction Approach With Turn-Off Delay Time for High-Voltage High-Power IGBT Modules," IEEE Trans. Power Electron., **31**(7), pp. 5122–5132.
[10] Chiu, Y. F., Tsai, Y. L., and Hwang, W. S., 2003, "Mathematical Modeling for the Solidification Heat-Transfer Phenomena During the Reflow Process of Lead-Tin Alloy Solder Joint in Electronics Packaging," Appl. Math. Modell., **27**(7), pp. 565–579.
[11] Liang, M.-W., Yen, H.-T., and Hsieh, T.-E., 2006, "Investigation of Electroless Cobalt-Phosphorous Layer and Its Diffusion Barrier Properties of Pb-Sn Solder," J. Electron. Mater., **35**(7), pp. 1593–1599.
[12] Kim, D., Nagao, S., Chen, C. T., Wakasugi, N., Yamamoto, Y., Suetake, A., Takemasa, T., Sugahara, T., and Suganuma, K., 2021, "Online Thermal Resistance and Reliability Characteristic Monitoring of Power Modules With Ag Sinter Joining and Pb, Pb-Free Solders During Power Cycling Test by SiC TEG Chip," IEEE Trans. Power Electron., **36**(5), pp. 4977–4990.
[13] Peng, J., Wang, M., Sadeghi, B., Wang, R. C., Liu, H. S., and Cavaliere, P., 2021, "Increasing Shear Strength of Au-Sn Bonded Joint Through Nano-Grained Interfacial Reaction Products," J. Mater. Sci., **56**(11), pp. 7050–7062.
[14] Yin, L. M., Lin, J. X., Zhang, T. T., Yao, Z. X., Du, C. H., and Tang, M., 2013, "Comparison of Mechanical Properties of Lead-Free Microscale Solder Joints Under Tensile and Shear Loading," 14th International Conference on Electronic Packaging Technology (ICEPT), IEEE, Dalian, China, Aug. 11–14.
[15] El-Daly, A. A., Mohamad, A. Z., Fawzy, A., and El-Taher, A. M., 2011, "Creep Behavior of Near-Peritectic Sn-5Sb Solders Containing Small Amount of Ag and Cu," Mater. Sci. Eng. A, **528**(3), pp. 1055–1062.
[16] Manikam, V. R., and Cheong, K. Y., 2011, "Die Attach Materials for High Temperature Applications: A Review," IEEE Trans. Compon. Packag. Manuf. Technol., **1**(4), pp. 457–478.
[17] Zhang, P., Jiang, X., Yuan, P., Yan, H., and Yang, D., 2018, "Silver Nanopaste: Synthesis, Reinforcements and Application," Int. J. Heat Mass Transfer, **127**, pp. 1048–1069.
[18] Zhang, S., Xu, X., Lin, T., and He, P., 2019, "Recent Advances in Nano-Materials for Packaging of Electronic Devices," J. Mater. Sci.-Mater. Electron., **30**(15), pp. 13855–13868.
[19] Lee, C. J., Bang, J. O., and Jung, S. B., 2019, "Effect of Black Residue on the Mechanical Properties of Sn-58Bi Epoxy Solder Joints," Microelectron. Eng., **216**(AUG), p. 111055.
[20] Sharma, A., Jung, D.-h., Cheon, J. S., and Jung, J.-P., 2019, "Epoxy Polymer Solder Pastes for Micro-Electronic Packaging Applications," J. Weld. Join., **37**(2), pp. 7–14.
[21] Sung, Y.-G., Myung, W.-R., Jeong, H., Ko, M.-K., Moon, J., and Jung, S.-B., 2018, "Mechanical Reliability of the Epoxy Sn-58 wt.%Bi Solder Joints With Different Surface Finishes Under Thermal Shock," J. Electron. Mater., **47**(7), pp. 4165–4169.
[22] Hwang, B.-U., Jung, K.-H., Min, K. D., Lee, C.-J., and Jung, S.-B., 2021, "Pressureless Cu-Cu Bonding Using Hybrid Cu-Epoxy Paste and Its Reliability," J. Mater. Sci.-Mater. Electron., **32**(3), pp. 3054–3065.
[23] Zou, G., Yan, J., Mu, F., Wu, A., and Zhou, Y. N., 2011, "Recent Progress in Microjoining and Nanojoining," Hanjie Xuebao/Trans. China Weld. Inst., **32**(4), pp. 107–112.
[24] Scheuermann, U., and Wiedl, P., 1997, "Low Temperature Joining Technology - A High Reliability Alternative to Solder Contacts," Workshop on Metal Ceramic Materials for Functional Applications, Wien, Austria, June 4–6, pp. 181–192.
[25] Jarosz, M., Jakubowska, M., Kielbasinski, K., Mlozniak, A., and Teodorczyk, M., 2012, "Low Temperature Joining Technique (LTJT) as an Alternative to Lead-Free Soldering for Die-Attach Applications," Fourth Electronic System-Integration Technology Conference, IEEE, Amsterdam, The Netherlands, Sept. 17–20, pp. 1–6.
[26] Bai, J. G., Yin, J., Zhang, Z., Lu, G. Q., and Van Wyk, J. D., 2007, "High-Temperature Operation of SiC Power Devices by Low-Temperature Sintered Silver Die-Attachment," IEEE Trans. Adv. Packag., **30**(3), pp. 506–510.
[27] Chew, L. M., Schmitt, W., Schwarzer, C., and Nachreiner, J., 2018, "Micro-Silver Sinter Paste Developed for Pressure Sintering on Bare Cu Surfaces Under Air or Inert Atmosphere," IEEE 68th Electronic Components and Technology Conference, San Diego, CA, May 29–June 1, pp. 323–330.
[28] Chua, S. T., and Siow, K. S., 2016, "Microstructural Studies and Bonding Strength of Pressureless Sintered Nano-Silver Joints on Silver, Direct Bond Copper (DBC) and Copper Substrates Aged at 300 °C," J. Alloys Compd., **687**, pp. 486–498.
[29] Mei, Y., Li, X., Ning, P., Fu, S., and Lu, G.-Q., 2015, "Parametric Study on Pressureless Sintering of Nanosilver Paste to Bond Large-Area (a Parts per Thousand yen100 mm(2)) Power Chips at Low Temperatures for Electronic Packaging," J. Electron. Mater., **44**(10), pp. 3973–3984.
[30] Schmitt, W., 2016, "Adjust the Mechanical Properties of Sintered Silver Layers Using Additives," Cips International Conference on Integrated Power Electronics Systems, IEEE, Nuremberg, Germany, Mar. 8–10, pp. 1–7.
[31] Schmitt, W., and Heraeus, W. C., 2010, "New Silver Contact Pastes From High Pressure Sintering to Low Pressure Sintering," Third Electronics System Integration Technology Conference (ESTC), IEEE, Berlin, Germany, Sept. 13–16, pp. 1–6.
[32] Stuckner, J. A., Lu, G. Q., Mitsuhara, M., Reynolds, W. T., and Murayama, M., 2017, "The Influence of Processing Conditions on the 3-D Interconnected Structure of Nanosilver Paste," IEEE Trans. Electron Devices, **64**(2), pp. 494–496.
[33] Duch, S., Krebs, T., Loewer, Y., Schmitt, W., and Thomas, M., and 2012, "Novel Interconnect Materials for High Reliability Power Converters With Operation Temperatures Above 150 °C," IEEE 62nd Electronic Components and Technology Conference, IEEE, San Diego, CA, May 29–June 1, pp. 416–422.
[34] Yang, Y., Yin, L. M., Xian, J. W., Xin, M. A., and Zhang, X. P., 2008, "Green Manufacturing of Electronics and Materials for Green Electronic Packaging," Electron. Process Technol., **29**(5), pp. 256–260.
[35] Manikam, V. R., and Tolentino, E. N., 2015, "Sintering of Ag Paste for Power Devices Die Attach on Cu Surfaces," IEEE 16th Electronics Packaging Technology Conference (EPTC), IEEE, Singapore, Dec. 3–5.
[36] Jung, K.-H., Min, K. D., Lee, C.-J., Park, B.-G., Jeong, H., Koo, J.-M., Lee, B., and Jung, S.-B., 2019, "Effect of Epoxy Content in Ag Nanoparticle Paste on the Bonding Strength of MLCC Packages," Appl. Surf. Sci., **495**, p. 143487.
[37] Dias, M., Costa, T. A., Silva, B. L., Spinelli, J. E., Cheung, N., and Garcia, A., 2018, "A Comparative Analysis of Microstructural Features, Tensile Properties and Wettability of Hypoperitectic and Peritectic Sn-Sb Solder Alloys," Microelectron. Reliab., **81**, pp. 150–158.
[38] Liu, Y., Zhang, H., Wang, L., Fan, X., Zhang, G., and Sun, F., 2018, "Effect of Sintering Pressure on the Porosity and the Shear Strength of the Pressure-Assisted Silver Sintering Bonding," IEEE Trans. Device Mater. Reliab., **18**(2), pp. 240–246.
[39] Kim, K. S., Park, B. G., Jung, K. H., Kim, J. W., Jeong, M. Y., and Jung, S. B., 2015, "Microwave Sintering of Silver Nanoink for Radio Frequency Applications," J. Nanosci. Nanotechnol., **15**(3), pp. 2333–2337.
[40] Schmitt, W., Chew, L. M., and Miller, R., 2018, "Pressure-Less Sintering on Large Dies Using Infrared Radiation and Optimized Silver Sinter Paste," IEEE 68th Electronic Components and Technology Conference, San Diego, CA, May 29–June 1, pp. 539–544.
[41] Peng, P., Hu, A., and Zhou, Y., 2012, "Laser Sintering of Silver Nanoparticle Thin Films: Microstructure and Optical Properties," Appl. Phys. A, **108**(3), pp. 685–691.
[42] Fang, H., Wang, C., Zhou, S., Kang, Q., Wang, T., Yang, D., Tian, Y., and Suga, T., 2020, "Rapid Pressureless and Low-Temperature Bonding of Large-Area Power Chips by Sintering Two-Step Activated Ag Paste," J. Mater. Sci.-Mater. Electron., **31**(8), pp. 6497–6505.
[43] Hong, W. S., Kim, M. S., and Hong, K.-K., 2021, "Electrical and Microstructural Reliability of Pressureless Silver-Sintered Joints on Silicon Carbide Power Modules Under Thermal Cycling and High-Temperature Storage," J. Electron. Mater., **50**(3), pp. 914–925.
[44] Watanabe, T., Takesue, M., Matsuda, T., Sano, T., and Hirose, A., 2020, "Thermal Stability and Characteristic Properties of Pressureless Sintered Ag Layers Formed With Ag Nanoparticles for Power Device Applications," J. Mater. Sci.-Mater. Electron., **31**(20), pp. 17173–17182.

Downloaded from http://asmedigitalcollection.asme.org/electronicpackaging/article-pdf/144/4/041013/6875569/ep_144_04_041013.pdf by Bibliotheek Tu Delft user on 05 January 2023